arXiv:1403.7929v1 [physics.med-ph] 31 Mar 2014

Comparative study of RBE and cell survival fractions for ^{1}H, ^{4}He, ^{12}C and ^{16}O beams using Geant4 and Microdosimetric Kinetic model

Lucas N Burigo*[1,2], Igor A Pshenichnov[1,3], Igor N Mishustin[1,4], and Marcus Bleicher[1,2]

[1]Frankfurt Institute for Advanced Studies, Johann Wolfgang Goethe University, 60438 Frankfurt am Main, Germany
[2]Institut für Theoretische Physik, Johann Wolfgang Goethe University, 60438 Frankfurt am Main, Germany
[3]Institute for Nuclear Research, Russian Academy of Sciences, 117312 Moscow, Russia
[4]Kurchatov Institute, Russian Research Center, 123182 Moscow, Russia

April 1, 2014

Abstract

Beams of ^{4}He and ^{16}O nuclei are considered for ion-beam cancer therapy as alternative options to protons and ^{12}C nuclei. Spread-out Bragg peak (SOBP) distributions of physical dose and relative biological effectiveness for 10% survival are calculated by means of our Geant4-based Monte Carlo model for Heavy Ion Therapy (MCHIT) and the modified microdosimetric kinetic model. The depth distributions of cell survival fractions are calculated for ^{1}H, ^{4}He, ^{12}C and ^{16}O for tissues with normal (HSG cells), low and high radiosensitivity. In each case the cell survival fractions were compared separately for the target volume, behind and in front of it. In the case of normal radiosensitivity ^{4}He and ^{12}C better spare tissues in the entrance channel compared to protons and ^{16}O. The cell survival fractions calculated, respectively, for the entrance channel and target volume are similar for ^{4}He and ^{12}C. When it is important to spare healthy tissues located after the distal edge of the SOBP plateau, ^{4}He can be recommended due to reduced nuclear fragmentation of these projectiles. No definite advantages of ^{16}O with respect to ^{12}C were found, with the except of an enhanced impact of these heavier projectiles on radioresistant tumors.

1 Introduction

The advantage of charged particles, in particular, protons and carbon nuclei, used for radiation therapy of cancer consists in elevated dose delivered at the end of projectile range in tissues. The plateau of the depth-dose distribution at the entrance of a monoenergetic beam terminates with a sharp Bragg peak which can be targeted at the tumor. Such a dose profile helps to spare healthy tissues located in front of the tumor as well as beyond the projectile range. Since a set of beam energies is typically used in treatments to cover the whole tumor volume, the resulting dose distribution is characterized by a spread-out Bragg peak (SOBP) [1, 2, 3] with a wide domain of elevated dose.

The damage of healthy tissues during therapy can be essentially reduced if the ratio between the relative biological effectiveness (RBE) values at the SOBP region and plateau is favorable. As recognized almost 40 years ago in radiobiological experiments with SOBP beams of light nuclei performed at Berkeley [4], this RBE ratio is greater than 1 and increases with ion charge up to carbon. It was also found that this ratio decreases for Ne and becomes less than 1. In 1994 first patient treatments with beams of carbon nuclei started in Japan at National Institute of Radiological Sciences (NIRS) [5] and in 1997 in Germany at Gesellschaft für Schwerionenforschung (GSI) [3]. Later the advantages of ^{12}C with respect to ^{3}He and ^{20}Ne were confirmed in experiments at NIRS with these nuclear beams [6]. As explained [7], the RBE of 135 MeV/u ^{12}C beam with the linear energy transfer (LET) of 65 keV/μm was found similar to the RBE of neutrons which have been used for treatment at NIRS during last

*Electronic address: burigo@fias.uni-frankfurt.de; Corresponding author

20 years. This similarity also motivated the choice of carbon nuclei for treatments at NIRS. In the last decades localized tumors have been successfully treated with beams of carbon nuclei at several facilities constructed in Japan and Germany [8, 9, 10, 11, 12, 13].

Despite of the broad clinical experience collected worldwide with proton and carbon-ion beams, other light nuclei can be also considered as future therapy options. The radiobiological properties of proton and ^{12}C beams were compared in several studies, see e.g. [14, 15]. However, less attention has been paid so far to ^{4}He or ^{16}O and to their comparison with protons and ^{12}C. There exist several clinical rationale behind the use of ^{4}He and ^{16}O for therapy:

i) ^{4}He and ^{16}O beams have a reduced lateral spread of the dose distribution compared to protons;

ii) their RBE in the target volume is higher compared to protons;

iii) lower dose in the tail region and lower RBE in the plateau is expected for ^{4}He compared to ^{12}C due to reduced nuclear fragmentation of ^{4}He;

iv) ^{16}O is a promising option for hypoxic tumors as it provides a higher dose averaged LET in the target volume compared to ^{12}C.

The choice of ion species and their energies at each new particle therapy facility [16, 17, 18] essentially depends on LET and RBE of the projectiles under consideration. The distributions of dose, LET and dose averaged LET of ^{1}H, ^{4}He, ^{6,7}Li, ^{8}Be, ^{10}B, ^{12}C, ^{14}N and ^{16}O nuclei of therapeutic energies were studied [19, 20] by means of Monte Carlo simulations with SHIELD-HIT and FLUKA codes, respectively. Similar distributions for ^{1}H, ^{3}He, ^{12}C, ^{20}Ne and ^{58}Ni were calculated [21] with the Geant4 toolkit to study their dependence on the ions mass, charge and energy. It was assumed [19] that ions with LET above 20 keV/μm should be used for efficient cancer therapy as such species induce on average two and more double strand breaks in DNA close to each other. However, as pointed out in the same work, this limit is not sharp and ought to vary with ion mass and charge. This indicates that the RBE of respective ions has to be additionally considered for an accurate comparison of their biological action. Indeed, as shown in our recent work [22], there is no direct correspondence between RBE and the frequency-mean linear energy $\bar{y}_f$, which represents LET, for monoenergetic beams of therapeutic energies. Similar RBE values were estimated [22] at the peak and plateau regions which are characterized, however, by very different $\bar{y}_f$.

As demonstrated [22], microdosimetry spectra for monoenergetic ^{1}H, ^{4}He, ^{7}Li and ^{12}C nuclei propagating in a water phantom can be accurately described with our Monte Carlo model for Heavy-Ion Therapy (MCHIT) [23], and this model coupled with the Microdosimetric Kinetic (MK) model [24, 25] can be used to calculate the respective RBE profiles. In the present work we evaluate ^{4}He and ^{16}O for cancer therapy as complementary options to ^{1}H and ^{12}C by considering the biological dose distribution with a 6 cm SOBP delivered by these four projectiles. This is an important prerequisite for planning radiobiological experiments with ^{4}He and ^{16}O SOBP beams and extending existing treatment planning systems to operation with ^{4}He and ^{16}O.

The experimental data [7] collected at HIMAC for the 6 cm SOBP obtained by the moderation of a 290 MeV/u ^{12}C beam are used as a reference. The results of microdosimetry simulations are validated by comparison with microdosimetry data collected for ^{1}H, ^{4}He and ^{12}C beams [25]. This makes possible to predict the RBE and cell survival profiles for ^{16}O beams and compare all four ion species in a common framework.

2 Materials and methods

2.1 Monte Carlo modeling of propagation of ions in water

With the Monte Carlo model for Heavy Ion Therapy (MCHIT) [26, 23] the propagation of accelerated protons and light nuclei of therapeutic energies in tissue-like media can be simulated. The model is based on the Geant4 toolkit [27, 28] and takes into account all major physics processes relevant to the interactions of beam particles with these materials. The Geant4 version 9.5 with patch 02 is used to build the present version of MCHIT, which also simulates the interactions of various particles with walled and wall-less Tissue Equivalent Proportional Counters (TEPC) thus providing respective microdosimetry distributions.

The ionization of atoms and multiple Coulomb scattering on nuclei of the media are the most important electromagnetic processes to simulate the energy loss and straggling of primary and secondary charged particles. Two predefined physics lists for electromagnetic processes are employed in MCHIT, namely, G4EmStd (which uses the "Standard Electromagnetic Physics Option 3") and

G4EmPen (which uses the Penelope models for low-energy processes). The low-energy thresholds for production of δ-electrons are 990 eV for G4EmStd and 100 eV for G4EmPen. However, in order to reduce the CPU time, cuts in range and energy thresholds for particle production are set differently for water, plastic of the TEPC wall and the TEPC sensitive volume filled with tissue-equivalent gas [29]. A customized physics list, G4EmPen+IonGas, which is based on G4EmPen and the models describing the ionization of gas media by ions, can be also used in calculations. As demonstrated [22], G4EmStd and G4EmPen provide statistically equivalent results for microdosimetry spectra, which agree well with the distributions measured for ^{4}He [30], excluding the domains of low linear energy, y <1 keV/µm, and around the maximum at y ∼15 keV/µm. However, the agreement between the data and calculations is improved when G4EmPen+IonGas is used. Therefore, G4EmPen+IonGas is involved in MCHIT also in the present work to simulate electromagnetic processes inside the TEPC volume.

A therapeutic nuclear beam is attenuated in tissues due to the loss of beam nuclei in nuclear fragmentation reactions, which generate secondary projectile and target fragments [23]. Nuclear reactions are taken into account in MCHIT to reproduce this effect. As shown [23], the build-up of secondary fragments produced by 200 MeV/u and 400 MeV/u ^{12}C beams is generally well described with a customized physics list based on the Light Ion Binary Cascade model (G4BIC) [31] coupled with the Fermi break-up model (G4FermiBreakUp) [32] responsible for subsequent decays of excited nuclear fragments created at the first fast stage of nucleus-nucleus collisions. In the present work G4BIC is used for proton, helium and lithium beams, while the Quantum Molecular Dynamics model (G4QMD) [33] is involved in simulations with carbon and oxygen beams. More details on the physics processes and respective Geant4 models involved in modeling with MCHIT are given in our recent publications [23, 29, 22].

2.2 Microdosimetry simulations and calculations of RBE for monoenergetic beams

The design and materials of specific TEPC models were thoroughly introduced in MCHIT. This made possible to simulate the microdosimetry spectra measured with a walled TEPC at several positions inside a water phantom irradiated by 185 MeV/u ^{7}Li and 300 MeV/u ^{12}C beams [34] and study the impact of nuclear fragmentation reactions on these spectra [29, 22]. The influence of the positioning of the TEPC with respect to the beam axis and the distortion of the spectra due to the pile-up of individual events were investigated. After correcting for such effects the calculated microdosimetry spectra agree well with the experimental data in general.

Following the validation of MCHIT for microdosimetry of monoenergetic ^{7}Li and ^{12}C beams [29, 22], this model is applied to microdosimetry of SOBP dose distributions considered in the present work. In the measurements performed at HIMAC with a 6 cm SOBP for 160 MeV ^{1}H, 150 MeV/u ^{4}He and 290 MeV/u ^{12}C [25] the data for frequency-mean lineal energy, $\bar{y}_f$, dose-mean lineal energy, $\bar{y}_d$, and saturation-corrected dose-mean lineal energy, y^* [35] were collected. The microdosimetry spectra were measured with a walled TEPC corresponding to a tissue-equivalent sphere of 1 µm in diameter.

According to the linear-quadratic (LQ) model the fraction of cells S survived after the impact of the radiation dose D is calculated as

$$S = \exp\left[-\alpha D - \beta D^2\right] . \tag{1}$$

Following the modified MK model [25] applied to human salivary gland (HSG) tumor cells the parameter α is estimated as

$$\alpha = \alpha_0 + \frac{\beta}{\rho \pi r_d^2} y^* , \tag{2}$$

with the constant term $\alpha_0 = 0.13$ Gy^{-1} representing the initial slope of the survival fraction curve in the limit of zero LET and $\beta = 0.05$ Gy^{-2}, ρ =1 g/cm^3 as the density of tissue and r_d =0.42 μm as the radius of a sub-cellular domain in the MK model. The dependence of the α-parameter of the linear-quadratic model on y^* rather than on $\bar{y}_d$ reflects the reduction of the RBE known as the saturation effect. It means that an excessive local energy deposition does not boost biological effects induced by high-LET particles [35]. As demonstrated [25], the same value of parameter $\beta = 0.05$ Gy^{-2} can be used to fit the data on S with Eq. (1) for X-rays and ions. This justifies the assumption of the MK model that β is independent of LET.

According to the LQ model the RBE$_{10}$ for 10% survival of HSG cells is calculated using the

following relation [36]:

$$\mathrm{RBE}_{10} = \frac{D_{10,R}}{D_{10}} = \frac{2\beta D_{10,R}}{\sqrt{\alpha^2 - 4\beta \ln(0.1)} - \alpha}, \tag{3}$$

where D_{10} is the 10% survival dose of ions and $D_{10,R} = 5.0$ Gy is the 10% survival dose of the reference radiation (200 kVp X-rays) for HSG cells [36]. Finally, the biological dose D_{bio} is calculated from RBE_{10} and physical dose:

$$D_{bio} = \mathrm{RBE}_{10}\ D. \tag{4}$$

2.3 Composing SOBP profiles from a library of pristine Bragg peaks

The computing time required for treatment planing in carbon-ion therapy can be reduced by using pre-computed libraries of dose and RBE distributions for monoenergetic beams [37, 38, 39]. The aim of the treatment planning is to find an optimum superposition of many beams with their individual energy, position and intensity in order to obtain the prescribed biological SOBP dose profile. It is expected that a similar approach will be also suitable for other therapeutic beams, like ^{4}He and ^{16}O. Therefore, we implemented a common algorithm to calculate the relative weights of pre-defined monoenergetic beams of ^{1}H, ^{4}He, ^{12}C and ^{16}O to obtain flat biological SOBP distributions for each projectile as a product of the physical dose and RBE calculated for mixed radiation field.

A library of depth-dose profiles and the corresponding microdosimetry spectra for different beam energies and nuclei were calculated by Monte Carlo simulations with MCHIT. They are used as input data for a procedure similar to one implemented at NIRS [7]. According to this procedure based on the theory of dual radiation action [40] the survival fraction of cells exposed to mixed radiation is calculated as:

$$S_{mix}(D) = \exp\left(-\alpha_{mix} D - \beta_{mix} D^2\right); \tag{5}$$

$$\alpha_{mix} = \sum f_i \alpha_i; \tag{6}$$

$$\sqrt{\beta_{mix}} = \sum f_i \sqrt{\beta_i}. \tag{7}$$

Here f_i is the weight coefficient (fraction) of the local physical dose of the ith monoenergetic beam which contribute to the total physical dose D, while α_i and β_i are the parameters of the LQ model specific to ith monoenergetic beam. The parameters α_i and β_i are calculated along the beam axis using MCHIT coupled with the modified MK model as described in Sec. 2.2. The resulting $\mathrm{RBE}_{10,mix}$ for the mixed radiation is calculated from the survival fraction of cells $S_{mix}(D)$ and it also depends on the depth. RBE_{10} and $\mathrm{RBE}_{10,mix}$ for the monoenergetic and SOBP (mixed) beams, respectively, are considered in the following. They account for the relative biological effectiveness corresponding to 10% survival of cells.

A dedicated algorithm to obtain f_i for a given biological SOBP was developed. It starts with the determination of the weight at the distal edge of the SOBP distribution and then calculates weights for less energetic beams by adjusting their contribution to provide a flat SOBP plateau.

3 Results and discussion

3.1 Pristine Bragg peaks

Simulation results for monoenergetic 152.7 MeV ^{1}H, 152.1 MeV/u ^{4}He, 290 MeV/u ^{12}C and 345.4 MeV/u ^{16}O beams are shown in Figure 1. The beam energies were chosen to place the Bragg peaks of all four beams at the depth of ∼161.8 mm.

As expected, the ^{12}C and ^{16}O beams deposit much higher energy at the Bragg peak compared to ^{1}H and ^{4}He. However, higher energy deposition by ^{12}C and ^{16}O is also observed at the entrance and tail region. Therefore, no clear advantages of therapeutic ^{12}C and ^{16}O beams with respect to ^{1}H and ^{4}He beams regarding healthy tissues can be inferred exclusively from the analysis of the considered depth-dose distributions.

The RBE_{10} profiles for the considered ^{1}H, ^{4}He, ^{12}C and ^{16}O beams are shown in the middle panel of Figure 1 and they differ from each other. The RBE_{10} for ^{12}C beam estimated from the parameters of a LQ fitting on survival curves of HSG cells with β fixed to 0.05 Gy^{-2} [25] is presented for comparison. The RBE_{10} profile for ^{12}C beam calculated with MCHIT coupled with the MK model agrees well with the profile which is also calculated with MK, but using the measured microdosimetry data on y^* [25]. A prominent difference between RBE_{10} profiles for ^{12}C and ^{16}O and the profile for ^{4}He is seen in the insert of Figure 1. The backward shift of the maximum of RBE_{10} of ^{12}C and ^{16}O with respect to

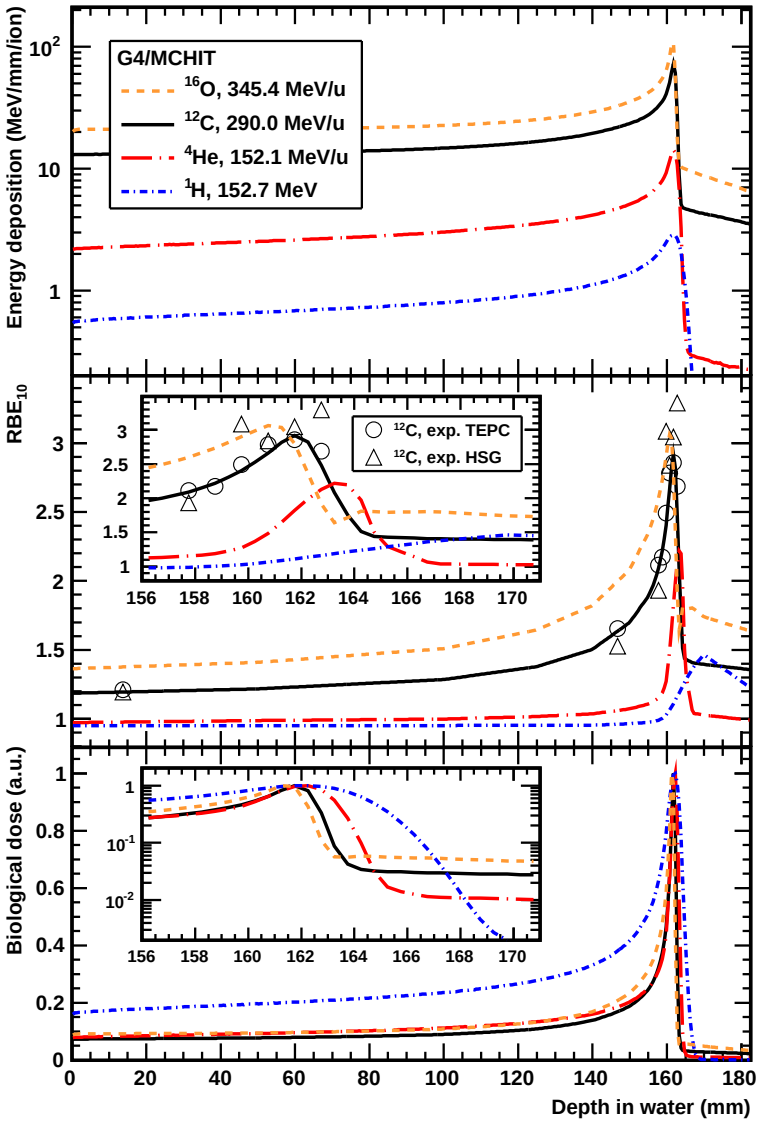

Figure 1: Calculated energy deposition per beam particle (top panel), RBE_{10} for HSG cells (middle panel) and biological dose (bottom panel) for ^{1}H, ^{4}He, ^{12}C and ^{16}O beams in water. The RBE_{10} calculated from measured values of y^* [25] are shown by circles. The RBE_{10} estimated from LQ fitting on survival curves of HSG cells [25] are presented by triangles. The biological dose distributions for all ions were rescaled to get the same value at the maximum.

the position of the ^{4}He maximum is due to the saturation effect. It is also found that ^{12}C and ^{16}O nuclei are characterized by higher RBE values for 10% survival of HSG cells along the whole irradiated medium. Their maximum values reach 2.9 and 3.1, respectively, close to the Bragg peak. At the same time the RBE_{10} values for helium are relatively low at the entrance and tail regions and demonstrate a steep rise to 2.2 at the Bragg peak position. Before the Bragg peak the RBE_{10} values for proton beam are slightly below 1. and increase to 1.5 well after the distal edge of the proton Bragg peak. This rise of RBE_{10} for proton beam is explained by the presence of secondary nucleons produced by beam protons in water and propagating beyond the Bragg peak.

Finally, the biological dose profiles for ^{1}H, ^{4}He, ^{12}C and ^{16}O (a.u.) are presented in the bottom panel of Figure 1. They were rescaled to get the same value at the maximum. The profiles for ^{4}He, ^{12}C and ^{16}O are very similar to each other. They are characterized by a more sharp rise and fall of the biological dose in the Bragg peak region compared to protons. After renormalization lower biological dose for ^{4}He, ^{12}C and ^{16}O is predicted at the entrance with respect to protons. SOBP profiles of biological dose for all these projectiles are considered below.

3.2 RBE distributions for ^{1}H, ^{4}He, ^{12}C and ^{16}O

As explained in Sec. 2.3, a given biological SOBP dose distribution is composed from a set of depth-dose and depth-y^* profiles calculated with MCHIT for monoenergetic beams. Such a library created in the present work contains pristine Bragg curves with a 1 mm increment of the Bragg peak positions which are within 90–175 mm depth in water. Seven pristine Bragg peaks for ^{12}C covering a 60 mm domain in depth are shown in Figure 2 to illustrate the content of this library. The microdosimetry variables which are also stored in the library as functions of depth are used to estimate RBE_{10} profiles according to the MK model, see Sec. 2.3. The respective RBE_{10} distributions are shown in Figure 2 for the same beams. As seen in Figure 2, the height of the Bragg peak noticeably diminishes with depth, while the maximum RBE_{10} remains almost constant (~ 3) over the considered depth range.

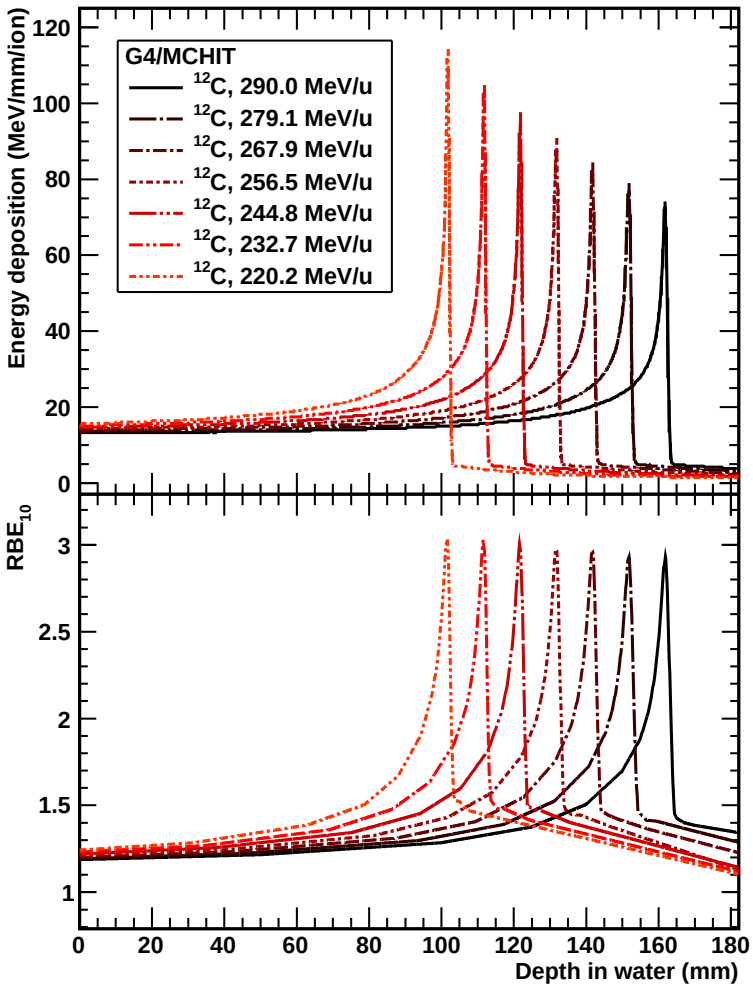

Figure 2: Energy deposition profiles for ^{12}C in water in 10 mm steps (top panel) and the corresponding RBE_{10} profiles for HSG cells calculated with MCHIT and the MK model (bottom panel).

A 6 cm-wide SOBP profile of biological dose for 290 MeV/u ^{12}C beam, which was built according to the above-described procedure is shown in the top panel of Figure 3. Here and in the following such profiles are normalized to 1 at the plateau in order to facilitate the comparison of various ion species. The resulting distribution has a flat SOBP plateau with negligible fluctuations due to the presence of individual Bragg peaks. In contrast, the corresponding SOBP distribution of the physical dose, which is also shown in Figure 3 is not flat, but rather decreases with depth. The respective RBE_{10} amounts to ~ 1.6 at the proximal edge of the SOBP, while it is slightly above 2.5 at the distal edge, see the bottom panel of Figure 3. The insert in the bottom panel of Figure 3 demonstrates the calculated relative weights for monoenergetic beams used to build the SOBP distribution of biological dose shown in Figure 3.

The 6 cm-wide $\mathrm{RBE}_{10,mix}$ profiles calculated for HSG cells for 152.7 MeV ^{1}H, 152.1 MeV/u ^{4}He, 290 MeV/u ^{12}C and 345.4 MeV/u ^{16}O beams are presented in Figure 4. They were calculated within the MK model basing on microdosimetry data generated by Monte Carlo simulations with MCHIT. The reliability of these profiles can be proved by comparing them with $\mathrm{RBE}_{10,mix}$ calculated by two

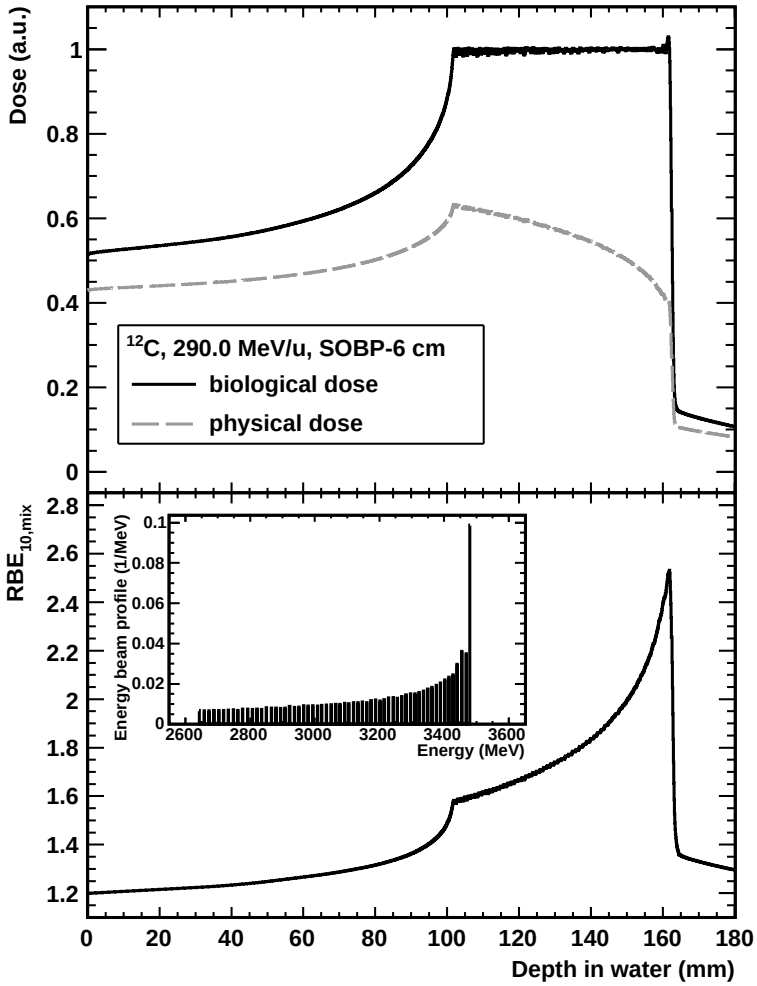

Figure 3: A 6 cm-wide SOBP biological dose distribution in water for 290 MeV/u ^{12}C ion beam and the respective physical dose (top panel). RBE$_{10,mix}$ profile for HSG cells (bottom panel) and the distribution of beam energy used to build the SOBP profiles (insert).

different approaches. In the first case, RBE$_{10,mix}$ is also calculated within the MK model, but on the basis of measured y^* values [25]. In the second approach, RBE$_{10,mix}$ is calculated using the parameters of LQ fitting of survival curves of HSG cells with β fixed to 0.05 Gy^{-2} [25]. The profiles based on MCHIT simulations agree very well with the RBE$_{10,mix}$ estimated on the basis of the two set of experimental data, see Figure 4. In order to make such comparison, experimental values [25] corresponding to ^{1}H and ^{4}He were shifted in depth due to the difference of beam energies used in measurements and simulations.

A good agreement with data for ^{1}H, ^{4}He and ^{12}C suggests that this method can be also applied to ^{16}O beam. The distribution of RBE$_{10,mix}$ for ^{16}O obtained on the basis of microdosimetry simulations with MCHIT is shown in Figure 4 for comparison. The shapes of RBE$_{10,mix}$ profiles for ^{4}He, ^{12}C and ^{16}O are found to be similar with a rise of RBE for ^{12}C and ^{16}O at the proximal edge of the SOBP distribution. A characteristic rise of RBE for ^{1}H beyond 165 mm depth at the distal region of the SOBP is found, similarly to the case of monoenergetic proton beam, Sec. 3.1. It is found that RBE$_{10,mix} \sim 1$ at the entrance region of ^{1}H and ^{4}He beams. The ratio between RBE$_{10,mix}$ values at the proximal (depth of $\sim$105 mm) and distal (depth of $\sim$165 mm) regions is larger for ^{16}O compared to ^{12}C. The RBE$_{10,mix}$ profile for ^{16}O demonstrates the most pronounced tail with respect to other projectiles.

3.3 SOBP distributions of biological dose

The SOBP distributions of biological dose D_{bio} for ^{1}H, ^{4}He, ^{12}C and ^{16}O are shown in Figure 5. They are calculated for HSG cell as a product of physical dose calculated with MCHIT and RBE$_{10,mix}$ obtained within the MK model on the basis of microdosimetric modeling with MCHIT. All four SOBP distributions presented in Figure 5 are 6 cm wide, and they are normalized to 1. at the plateau to

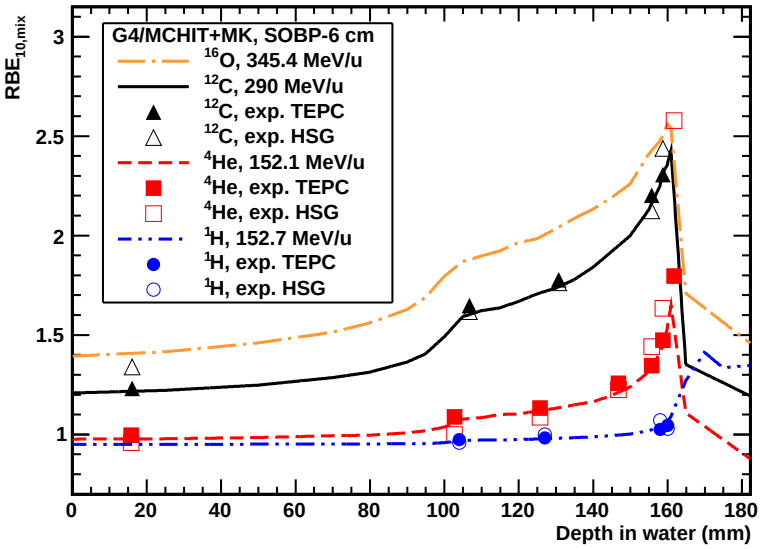

Figure 4: $\mathrm{RBE}_{10,mix}$ distributions calculated with MCHIT and the MK model for 6 cm SOBP beams of ^{1}H, ^{4}He, ^{12}C and ^{16}O. The beam energy profiles for ^{1}H, ^{4}He and ^{16}O were defined in such a way that they yield a 6 cm SOBP at the same depth as for 290 MeV/u ^{12}C ion. The $\mathrm{RBE}_{10,mix}$ values estimated with the MK model from measured y^* [25] are presented by full symbols as explained in the legend. The $\mathrm{RBE}_{10,mix}$ values estimated from LQ fitting of survival curves of HSG cells are presented by open symbols.

facilitate the comparison of their shapes and ratios between the plateau and entry channel. Therefore, in the following the distributions of D_{bio} are discussed in terms of dose relative to the plateau values.

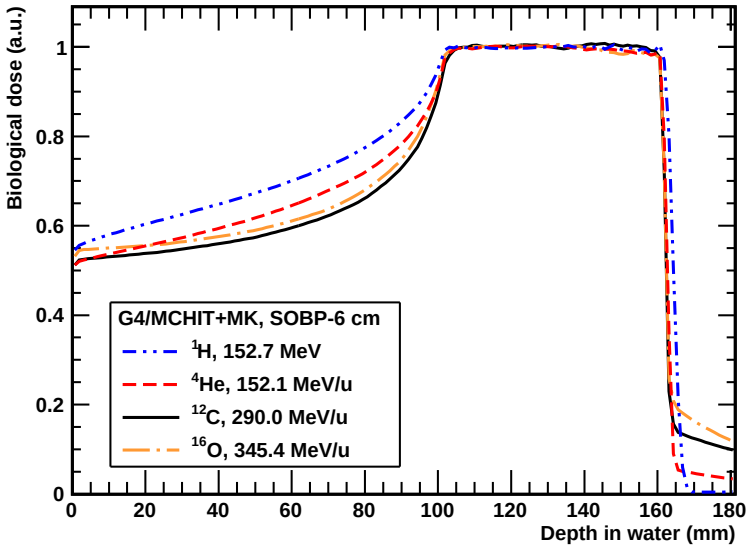

Figure 5: SOBP biological dose profiles for ^{1}H, ^{4}He, ^{12}C and ^{16}O nuclei obtained as a product of physical dose calculated with MCHIT and $\mathrm{RBE}_{10,mix}$ shown in Figure 4. The distributions for all projectiles were rescaled to get the same value at the plateau.

The distribution of D_{bio} for ^{12}C is characterized by the lowest values at the entrance channel. This helps to spare healthy tissues located in front of the target volume in treatments with ^{12}C. In contrast, the highest entrance dose is predicted for protons. However, the tail of the proton distribution beyond the distal edge of the plateau is negligible, while it is essential both for ^{12}C and ^{16}O. This indicates that the proton beam is the best option if very sensitive organs are located behind the tumor volume. The choice of ion species for each specific treatment can, in principle, provide an optimal ratio between the doses in the entrance and tail regions.

The distribution of D_{bio} for ^{4}He demonstrates a favorably small dose at the tail region, while its

entrance value is higher compared to ^{12}C. The biological dose delivered by ^{16}O to normal tissue is slightly increased both in front of the target volume and behind it compared to ^{12}C. From the analysis of D_{bio} distributions one can conclude that ^{12}C is the best treatment option compared to ^{1}H, ^{4}He and ^{16}O, unless only a very low D_{bio} is acceptable in the tail region. In the latter case protons become the best treatment option.

3.4 Distributions of cell survival fractions

The central part of our study is devoted to the comparison of survival fractions of cells S_{mix} calculated as a function of depth in the water phantom, which are estimated for tissues of different radiosensitivity. This makes possible to evaluate the respective therapeutic outcome for such tissues.

The distributions of S_{mix} calculated for cells (tissues) with $(\alpha/\beta)_{X-rays}$ = 3.8. Gy, 2 Gy and 10 Gy after exposing them to ^{1}H, ^{4}He, ^{12}C and ^{16}O SOBP beams are shown in Figure 6. Throughout this text the parameters for HSG cells were taken as $\alpha_0 = 0.13$ Gy^{-1} and $(\alpha/\beta)_{X-rays} = 3.8$. Gy [25]. Hereafter the radiosensitivity of such tissues is considered as normal. This serves as a natural reference point for comparison with two other tissues with their parameters taken following Kase *et al.* [41]. The latter two cases correspond to early responding tissue ($\alpha_0 = 0.44$ Gy^{-1}, $(\alpha/\beta)_{X-rays} = 2$ Gy) very sensitive to radiation and late responding tissue ($\alpha_0 = 0.04$ Gy^{-1}, $(\alpha/\beta)_{X-rays} = 10$ Gy) which is radioresistant.

The dose applied to HSG cells (normal radiosensitivity) leads to their 10% survival at the target volume for all four beams. The beams of ^{4}He and ^{12}C equally well spare tissue in the entrance channel, while the impact of ^{1}H and ^{16}O is stronger there. As one can expect, the main difference between light ^{1}H, ^{4}He and heavier ^{12}C, ^{16}O is revealed beyond the distal edge of SOBP profile due to the tail of secondary fragments from ^{12}C and ^{16}O. One can also note that ^{16}O is the worst option for HSG cells, while ^{4}He is the best one.

In the case of early and late responding tissues, see Figure 6, middle and bottom panels, the relation between the survival fractions estimated for ^{1}H, ^{4}He, ^{12}C and ^{16}O beyond the distal edge of the SOBP plateau are quite similar to the case of HSG cells. This is because of the fact that the dose in the tail region is defined by the presence of secondary fragments, which is essential for ^{12}C and ^{16}O beams. In the case of early responding tissues less than 5% of cells survive in the tumor volume, but their survival outside it is also unacceptably low (10–20%). This means that in this case there are no advantages of charged particle therapy with respect to the intensity modulated radiation therapy (IMRT) with photons.

In the case of late responding tissues more cells ($\sim$ 15%) survive in the tumor volume after the impact of ^{1}H, ^{4}He, ^{12}C and ^{16}O SOBP beams, see Figure 6, bottom panel. The ^{12}C and ^{16}O SOBP beams are very effective in killing tumor cells, but the cell survival is also lower in the entrance channel ($\sim$ 40%) compared to $\sim$ 50% for ^{1}H and ^{4}He. By considering all three sensitivity cases one can conclude that the ^{4}He beam is equally suitable for irradiation of tissues with normal and low radiosensitivity as the ^{12}C beam. Moreover, due to the reduced fragmentation of ^{4}He, this option can be even better than ^{12}C when sparing tissues after the tumor volume is crucial. At the same time the ^{16}O beam has no clear advantages compared to ^{12}C. Due to higher ionization in the entrance channel and enhanced fragmentation more cells are killed by ^{16}O beam outside the tumor volume compared to ^{12}C beam. However, one can consider ^{16}O is a good option for highly resistant tumors, as it effectively kills cells in the tumor volume.

4 Conclusions

In this work we presented our approach based on Monte Carlo simulations of microdosimetric spectra of monoenergetic beams of ^{1}H, ^{4}He, ^{12}C and ^{16}O in water. It provides y^* values as input to the modified MK model [36] for calculating RBE$_{10,mix}$ for HSG cells for SOBP distributions composed from monoenergetic beams of these projectiles. This method gives RBE$_{10,mix}$ for ^{1}H, ^{4}He, ^{12}C which are in full agreement with RBE$_{10,mix}$ also calculated within the MK model, but from measured y^* [25] and RBE$_{10,mix}$ calculated from the parameters of LQ fitting of survival curves of HSG cells [25]. This makes us confident in extending our approach to ^{16}O beams for which the respective data are not available. Our approach provides well-adjusted biological dose distributions for ^{1}H, ^{4}He, ^{12}C and ^{16}O with a very flat SOBP plateau. Thus basic properties of mixed radiation fields in treatments with these projectiles are emulated.

It is found that the shapes of RBE$_{10,mix}$ profiles for ^{4}He, ^{12}C and ^{16}O are similar to each other, while the RBE$_{10,mix}$ for protons is almost constant ($\sim$ 1.) over the whole depth in water, excluding enhanced RBE$_{10,mix}$ ($\sim$ 1.2) after the distal edge of the SOBP plateau. Considerably lower RBE$_{10,mix}$

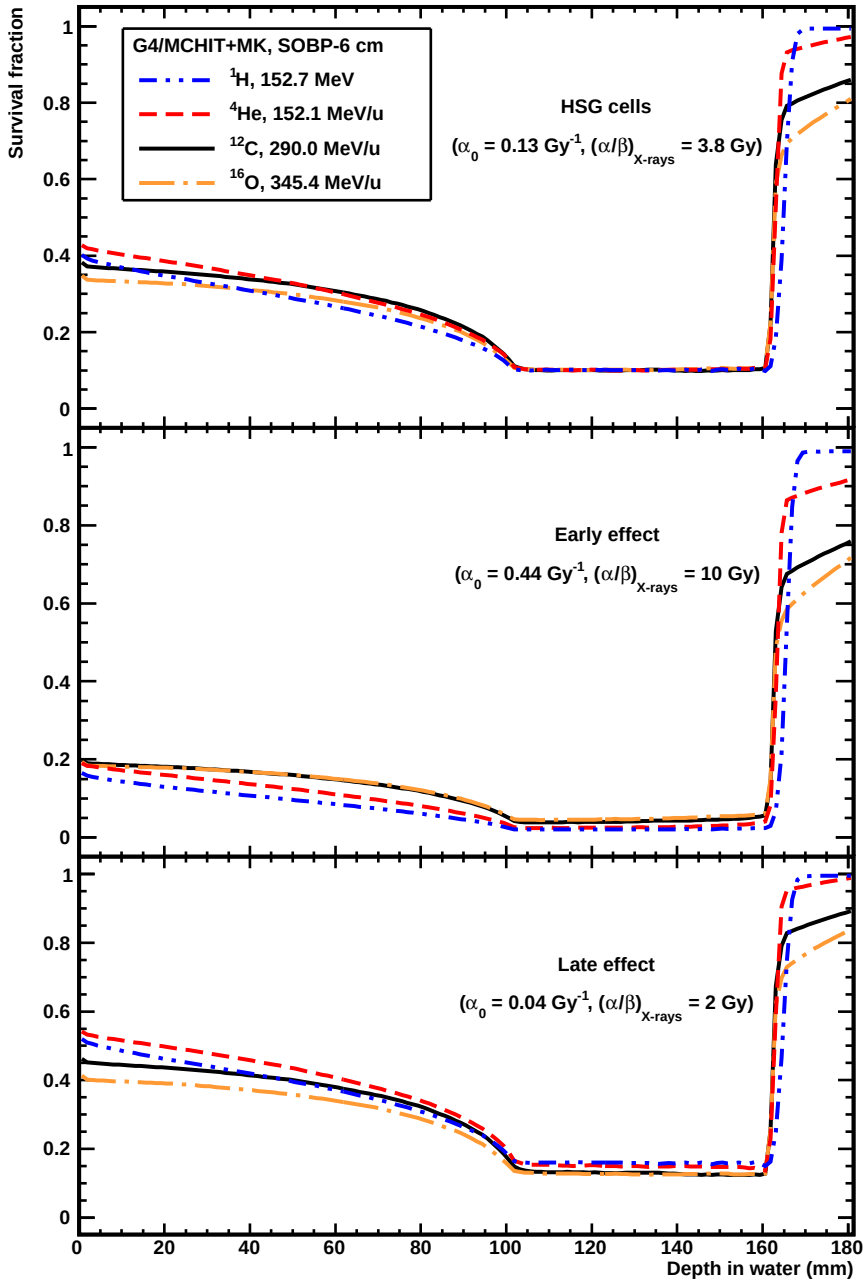

Figure 6: Distributions of cell survival rates S_{mix} after irradiation with ^{1}H, ^{4}He, ^{12}C and ^{16}O SOBP beams calculated for tissues with $(\alpha/\beta)_{X-rays}$ = 3.8. Gy (HSG cells, top panel), 2 Gy (early responding tissue, middle panel) and 10 Gy (late responding tissue, bottom panel). The values of α_0 parameter of the MK model are taken as 0.13 Gy^{-1}, 0.44 Gy^{-1} and 0.04 Gy^{-1}, respectively.

values are estimated in the entrance and tail region for ^{4}He compared to ^{12}C and ^{16}O. In the target volume the highest $\mathrm{RBE}_{10,mix}$ values of 1.5–2.5 are calculated for ^{12}C and ^{16}O.

In order to reduce side effects of ion therapy such as radionecrosis [41] the damage to surrounding healthy tissues should be reduced as much as possible. With the help of our MCHIT model connected with the modified MK model the severity of this damage is evaluated by calculating the cell survival fractions in healthy tissues for several kinds of therapeutic beams (^{1}H, ^{4}He, ^{12}C, ^{16}O). We considered the cases of normal (HSG cells), high and low radiosensitivity of tissues in the tumor volume and around it. The consideration of the impact of ^{1}H, ^{4}He, ^{12}C and ^{16}O SOBP beams in these three cases led us to the following conclusions:

- In the case of early responding tissues all four charged particle beams induce severe damage not only to the target volume, but also around it. Since in this case the region of high damage is not conformal to the target volume, the treatment with charged particles loses its advantages with respect to treatment with photons.

- In the case of tissues with normal radiosensitivity (HSG cells) ^{4}He and ^{12}C beams spare tissue in the entrance channel better than ^{1}H and ^{16}O ones.
- ^{4}He and ^{12}C nuclei are equally suitable for irradiation of tissues with normal and low radiosensitivity. The cell survival fractions calculated, respectively, for the entrance channel and target volume are similar for ^{4}He and ^{12}C.
- However, as soon as it is important to spare healthy tissues after the distal edge of the SOBP plateau, ^{4}H can be recommended due to the reduced nuclear fragmentation of these projectiles.
- No definitive advantages of ^{16}O with respect to ^{12}C were found, with the except of an enhanced impact of these heavier projectiles on radioresistant tumors.

In a recent work [42] the authors studied the possibility to spare healthy tissues by properly selecting ion species for therapy. In addition to ^{1}H, ^{4}He, ^{12}C they considered lithium, beryllium, boron and neon ions and calculated the dose to normal tissue delivered by these beams. However, the option of ^{16}O was not considered, while the Heidelberger Ionenstrahl-Therapiezentrum (HIT) in Heildeberg, Germany, provides ^{16}O beams of therapeutic energies [43, 11] in addition to ^{1}H, ^{4}He, ^{12}C. Treatments at this facility are performed presently only with protons and carbon ions, but ^{16}O can be also used following respective pre-clinical studies. In this sense our study complements the results of Remmes *et al.* [42] by considering ^{16}O beams, and also by comparing cell survival profiles in ^{1}H, ^{4}He, ^{12}C and ^{16}O treatments in addition to biological dose profiles.

As suggested [44], multi modal irradiations with various nuclei can be used for LET-painting. In this method high-LET radiation is used to boost the LET in a hypoxic sub-volume of the target (hypoxic compartments of the tumor). At the same time low-LET radiation is applied to the complementary target volume. Such combination may increase tumor control and reduce side effects. This means that a thorough evaluation of the physical properties and biological effectiveness of different beams is necessary before they can be applied in real treatments. Our approach can be also used for estimating RBE and cell survival fractions for ^{7}Li, ^{8}Be, ^{10}B and ^{14}N nuclei prior to planning radiobiological experiments with these beams.

Acknowledgements

This work was partially supported by HIC for FAIR within the Hessian LOEWE-Initiative. Our calculations were performed at the Center for Scientific Computing (CSC) of the Goethe University Frankfurt. We are grateful to the CSC staff for support.

References

[1] Yuki Kase, Nobuyuki Kanematsu, Tatsuaki Kanai, and Naruhiro Matsufuji. Biological dose calculation with monte carlo physics simulation for heavy-ion radiotherapy. *Phys. Med. Biol.*, 51(24):N467–N475, DEC 21 2006.

[2] John Gueulette and Andre Wambersie. Comparison of the methods of specifying carbon ion doses at nirs and gsi. *JOURNAL OF RADIATION RESEARCH*, 48(A):A97–A102, MAR 2007. NIRS-CNAO Joint Symposium on Carbon Ion Radiotherapy, Milan, ITALY, NOV 27-28, 2006.

[3] Dieter Schardt, Thilo Elsaesser, and Daniela Schulz-Ertner. Heavy-ion tumor therapy: Physical and radiobiological benefits. *Rev. Mod. Phys.*, 82(1):383–425, JAN-MAR 2010.

[4] J.D. Chapman, E.A. Blakely, K.C. Smith, and R.C. Urtasun. Radiobiological characterization of the inactivating events produced in mammalian cells by helium and heavy ions. *Int. J. Radiat. Oncol.*, 3:97 – 102, 1977. Particles and Radiation Therapy Second International Conference.

[5] Tatsuaki Kanai, Masahiro Endo, Shinichi Minohara, Nobuyuki Miyahara, Hiroko Koyama-ito, Hiromi Tomura, Naruhiro Matsufuji, Yasuyuki Futami, Akifumi Fukumura, Takeshi Hiraoka, Yoshiya Furusawa, Koichi Ando, Masao Suzuki, Fuminori Soga, and Kiyomitsu Kawachi. Biophysical characteristics of {HIMAC} clinical irradiation system for heavy-ion radiation therapy. *Int. J. Radiat. Oncol.*, 44(1):201 – 210, 1999.

[6] Y Furusawa, K Fukutsu, M Aoki, H Itsukaichi, K Eguchi-Kasai, H Ohara, E Yatagai, T Kanai, and K Ando. Inactivation of aerobic and hypoxic cells from three different cell lines by accelerated he-3-,c-12- and ne-20-ion beams. *RADIATION RESEARCH*, 154(5):485–496, NOV 2000.

[7] Naruhiro Matsufuji, Tatsuaki Kanai, Nobuyuki Kanematsu, Tadaaki Miyamoto, Masayuki Baba, Tadashi Kamada, Hirotoshi Kato, Shigeru Yamada, Jun-etsu Mizoe, and Hirohiko Tsujii. Specification of carbon ion dose at the national institute of radiological sciences (nirs). *JOURNAL OF RADIATION RESEARCH*, 48(A):A81–A86, MAR 2007. NIRS-CNAO Joint Symposium on Carbon Ion Radiotherapy, Milan, ITALY, NOV 27-28, 2006.

[8] Hirohiko Tsujii, Jun etsu Mizoe, Tadashi Kamada, Masayuki Baba, Shingo Kato, Hirotoshi Kato, Hiroshi Tsuji, Shigeru Yamada, Shigeo Yasuda, Tatsuya Ohno, Takeshi Yanagi, Azusa Hasegawa, Toshiyuki Sugawara, Hidefumi Ezawa, Susumu Kandatsu, Kyosan Yoshikawa, Riwa Kishimoto, and Tadaaki Miyamoto. Overview of clinical experiences on carbon ion radiotherapy at {NIRS}. *Radiotherapy and Oncology*, 73, Supplement 2:S41 – S49, 2004. Carbon-Ion Theraphy Proceedings of the Heavy Charged Particles in Biology and Medecine.

[9] Daniela Schulz-Ertner and Hirohiko Tsujii. Particle radiation therapy using proton and heavier ion beams. *JOURNAL OF CLINICAL ONCOLOGY*, 25(8):953–964, MAR 10 2007.

[10] Marco Durante and Jay S. Loeffler. Charged particles in radiation oncology. *Nat. Rev. Clin. Oncol.*, 7(1):37–43, JAN 2010.

[11] Stephanie E. Combs, Oliver Jäkel, Thomas Haberer, and Jürgen Debus. Particle therapy at the heidelberg ion therapy center (hit) – integrated research-driven university-hospital-based radiation oncology service in heidelberg, germany. *Radiotherapy and Oncology*, 95(1):41 – 44, 2010.

[12] A. D. Jensen, M. W. Muenter, and J. Debus. Review of clinical experience with ion beam radiotherapy. *Brit. J. Radiol.*, 84(1):S35–S47, DEC 2011.

[13] Tadashi Kamada. Clinical evidence of particle beam therapy (carbon). *Int. J. Clin. Oncol.*, 17(2):85–88, APR 2012.

[14] Jan J. Wilkens and Uwe Oelfke. Direct comparison of biologically optimized spread-out bragg peaks for protons and carbon ions. *Int. J. Radiat. Oncol.*, 70(1):262 – 266, 2008.

[15] Herman Suit, Thomas DeLaney, Saveli Goldberg, Harald Paganetti, Ben Clasie, Leo Gerweck, Andrzej Niemierko, Eric Hall, Jacob Flanz, Josh Hallman, and Alexei Trofimov. Proton vs carbon ion beams in the definitive radiation treatment of cancer patients. *Radiotherapy and Oncology*, 95(1):3 – 22, 2010.

[16] A Brahme, R Lewensohn, U Ringborg, U Amaldi, F Gerardi, and S Rossi. Design of a centre for biologically optimised light ion therapy in stockholm. *Nucl. Instrum. Methods B*, 184(4):569 – 588, 2001.

[17] Hans Svensson, Ulrik Ringborg, Ingemar Naeslund, and Anders Brahme. Development of light ion therapy at the karolinska hospital and institute. *Radiotherapy and Oncology*, 73, Supplement 2:S206 – S210, 2004. Carbon-Ion Theraphy Proceedings of the Heavy Charged Particles in Biology and Medecine.

[18] J Lundkvist, M Ekman, SR Ericsson, B Jonsson, and B Glimelius. Proton therapy of cancer: Potential clinical advantages and cost-effectiveness. *ACTA ONCOLOGICA*, 44(8):850–861, DEC 2005.

[19] Johanna Kempe, Irena Gudowska, and Anders Brahme. Depth absorbed dose and let distributions of therapeutic h-1, he-4, li-7, and c-12 beams. *Med. Phys.*, 34(1):183–192, JAN 2007.

[20] I. Kantemiris, P. Karaiskos, P. Papagiannis, and A. Angelopoulos. Dose and dose averaged let comparison of h-1, he-4, li-6, be-8, b-10, c-12, n-14, and o-16 ion beams forming a spread-out bragg peak. *Med. Phys.*, 38(12):6585–6591, DEC 2011.

[21] Igor Pshenichnov, Igor Mishustin, and Walter Greiner. Comparative study of depth-dose distributions for beams of light and heavy nuclei in tissue-like media. *Nucl. Instrum. Methods B*, 266(7):1094–1098, APR 2008.

[22] Lucas Burigo, Igor Pshenichnov, Igor Mishustin, and Marcus Bleicher. Microdosimetry spectra and rbe of ^{1}h, ^{4}he, ^{7}li and ^{12}c nuclei in water studied with geant4. *Nucl. Instrum. Methods B*, 320:89 – 99, 2014.

[23] Igor Pshenichnov, Alexander Botvina, Igor Mishustin, and Walter Greiner. Nuclear fragmentation reactions in extended media studied with geant4 toolkit. *Nucl. Instrum. Methods B*, 268(6):604–615, MAR 15 2010.

[24] Roland B. Hawkins. A microdosimetric-kinetic model for the effect of non-poisson distribution of lethal lesions on the variation of rbe with let. *Radiation Research*, 160(1):61–69, JUL 2003.

[25] Yuki Kase, Tatsuaki Kanai, Yoshitaka Matsumoto, Yoshiya Furusawa, Hiroyuki Okamoto, Toru Asaba, Makoto Sakama, and Hiroshi Shinoda. Microdosimetric measurements and estimation of human cell survival for heavy-ion beams. *Radiat. Res.*, 166(4):629–638, OCT 2006.

[26] I. Pshenichnov, I. Mishustin, and W Greiner. Neutrons from fragmentation of light nuclei in tissue-like media: a study with the geant4 toolkit. *Phys. Med. Biol.*, 50(23):5493–5507, 2005.

[27] S Agostinelli, J Allison, K Amako, J Apostolakis, H Araujo, P Arce, M Asai, D Axen, S Banerjee, G Barrand, F Behner, L Bellagamba, J Boudreau, L Broglia, A Brunengo, H Burkhardt, S Chauvie, J Chuma, R Chytracek, G Cooperman, G Cosmo, P Degtyarenko, A Dell'Acqua, G Depaola, D Dietrich, R Enami, A Feliciello, C Ferguson, H Fesefeldt, G Folger, F Foppiano, A Forti, S Garelli, S Giani, R Giannitrapani, D Gibin, JJG Cadenas, I Gonzalez, GG Abril, G Greeniaus, W Greiner, V Grichine, A Grossheim, S Guatelli, P Gumplinger, R Hamatsu, K Hashimoto, H Hasui, A Heikkinen, A Howard, V Ivanchenko, A Johnson, FW Jones, J Kallenbach, N Kanaya, M Kawabata, Y Kawabata, M Kawaguti, S Kelner, P Kent, A Kimura, T Kodama, R Kokoulin, M Kossov, H Kurashige, E Lamanna, T Lampen, V Lara, V Lefebure, F Lei, M Liendl, W Lockman, F Longo, S Magni, M Maire, E Medernach, K Minamimoto, PM de Freitas, Y Morita, K Murakami, M Nagamatu, R Nartallo, P Nieminen, T Nishimura, K Ohtsubo, M Okamura, S O'Neale, Y Oohata, K Paech, J Perl, A Pfeiffer, MG Pia, F Ranjard, A Rybin, S Sadilov, E Di Salvo, G Santin, T Sasaki, N Savvas, Y Sawada, S Scherer, S Seil, V Sirotenko, D Smith, N Starkov, H Stoecker, J Sulkimo, M Takahata, S Tanaka, E Tcherniaev, ES Tehrani, M Tropeano, P Truscott, H Uno, L Urban, P Urban, M Verderi, A Walkden, W Wander, H Weber, JP Wellisch, T Wenaus, DC Williams, D Wright, T Yamada, H Yoshida, and D Zschiesche. Geant4-a simulation toolkit. *Nucl. Instrum. Methods A*, 506(3):250–303, JUL 1 2003.

[28] J Allison, K Amako, J Apostolakis, H Araujo, PA Dubois, M Asai, G Barrand, R Capra, S Chauvie, R Chytracek, GAP Cirrone, G Cooperman, G Cosmo, G Cuttone, GG Daquino, M Donszelmann, M Dressel, G Folger, F Foppiano, J Generowicz, V Grichine, S Guatelli, P Gumplinger, A Heikkinen, I Hrivnacova, A Howard, S Incerti, V Ivanchenko, T Johnson, F Jones, T Koi, R Kokoulin, M Kossov, H Kurashige, V Lara, S Larsson, F Lei, O Link, F Longo, M Maire, A Mantero, B Mascialino, I McLaren, PM Lorenzo, K Minamimoto, K Murakami, P Nieminen, L Pandola, S Parlati, L Peralta, J Perl, A Pfeiffer, MG Pia, A Ribon, P Rodrigues, G Russo, S Sadilov, G Santin, T Sasaki, D Smith, N Starkov, S Tanaka, E Tcherniaev, B Tome, A Trindade, P Truscott, L Urban, M Verderi, A Walkden, JP Wellisch, DC Williams, D Wright, and H Yoshida. Geant4 developments and applications. *IEEE T. Nucl. Sci.*, 53(1, Part 2):270–278, FEB 2006.

[29] Lucas Burigo, Igor Pshenichnov, Igor Mishustin, and Marcus Bleicher. Microdosimetry of radiation field from a therapeutic ^{12}c beam in water: A study with geant4 toolkit. *Nucl. Instrum. Methods B*, 310:37 – 53, 2013.

[30] Shuichi Tsuda, Tatsuhiko Sato, Fumiaki Takahashi, Daiki Satoh, Shinichi Sasaki, Yoshihito Namito, Hiroshi Iwase, Shuichi Ban, and Masashi Takada. Systematic measurement of lineal energy distributions for proton, he and si ion beams over a wide energy range using a wall-less tissue equivalent proportional counter. *J. Radiat. Res.*, 53(2):264–271, 2012.

[31] G. Folger, V.N. Ivanchenko, and J.P. Wellisch. The binary cascade. *The European Physical Journal A - Hadrons and Nuclei*, 21(3):407–417, 2004.

[32] JP Bondorf, AS Botvina, AS Iljinov, IN Mishustin, and K Sneppen. Statistical multifragmentation of nuclei. *Phys. Rep.*, 257(3):133–221, JUN 1995.

[33] T Koi. New native qmd code in geant4. *Proceedings of the MC2010 Monte Carlo Conference*, 2010.

[34] G. Martino, M. Durante, and D. Schardt. Microdosimetry measurements characterizing the radiation fields of 300 mev/u (12)c and 185 mev/u (7)li pencil beams stopping in water. *Phys. Med. Biol.*, 55(12):3441–3449, JUN 21 2010.

[35] "International Commission of Radiation Units and Measurements (ICRU)". *Microdosimetry.* Report No 36 (Bethesda, MD), 1983.

[36] Yuki Kase, Tatsuaki Kanai, Makoto Sakama, Yuji Tameshige, Takeshi Himukai, Hiroyuki Nose, and Naruhiro Matsufuji. Microdosimetric approach to nirs-defined biological dose measurement for carbon-ion treatment beam. *J. Radiat. Res.*, 52(1):59–68, JAN 2011.

[37] M Krämer, O Jäkel, T Haberer, G Kraft, D Schardt, and U Weber. Treatment planning for heavy-ion radiotherapy: physical beam model and dose optimization. *Phys. Med. Biol.*, 45(11):3299–3317, NOV 2000.

[38] M Krämer and M Scholz. Treatment planning for heavy-ion radiotherapy: calculation and optimization of biologically effective dose. *Phys. Med. Biol.*, 45(11):3319–3330, NOV 2000.

[39] O Jäkel, M Krämer, CP Karger, and J Debus. Treatment planning for heavy ion radiotherapy: clinical implementation and application. *Phys. Med. Biol.*, 46(4):1101–1116, APR 2001.

[40] M. Zaider and H. H. Rossi. The synergistic effects of different radiations. *Radiat. Res.*, 83(3):732–739, 1980.

[41] Yuki Kase, Takeshi Himukai, Ai Nagano, Yuji Tameshige, Shinichi Minohara, Naruhiro Matsufuji, Junetsu Mizoe, Piero Fossati, Azusa Hasegawa, and Tatsuaki Kanai. Preliminary calculation of rbe-weighted dose distribution for cerebral radionecrosis in carbon-ion treatment planning. *J. Radiat. Res.*, 52(6):789–796, NOV 2011.

[42] Nicholas B Remmes, Michael G Herman, and Jon J Kruse. Optimizing normal tissue sparing in ion therapy using calculated isoeffective dose for ion selection. *Int. J. Radiat. Oncol.*, 83:756–762, 2012.

[43] Th. Haberer, J. Debus, H. Eickhoff, O. Jäkel, D. Schulz-Ertner, and U. Weber. The heidelberg ion therapy center. *Radiotherapy and Oncology*, 73, Supplement 2:S186 – S190, 2004. Carbon-Ion Theraphy Proceedings of the Heavy Charged Particles in Biology and Medecine.

[44] Niels Bassler, Oliver Jäkel, Christian Skou Søndergaard, and Jørgen B. Petersen. Dose- and let-painting with particle therapy. *Acta Oncologica*, 49(7):1170–1176, 2010.